# A PAH growth mechanism and effect of alcohol addition on PAH formation in counterflow ethylene diffusion flames

Sungwoo Park[1,*], Yu Wang[1], Suk Ho Chung[1], S. Mani Sarathy[1]

[1]Clean Combustion Research Center, King Abdullah University of Science and Technology, Thuwal, Kingdom of Saudi Arabia

**Abstract**

This study presents a chemical kinetic model for ethylene/alcohol flames with polycyclic aromatic hydrocarbons (PAHs) growth up to A7 (coronene, $C_{24}H_{12}$). In order to take into account recent kinetic investigations, the KAUST PAH sub-mechanism was merged with NUIG's $C_0$-$C_3$ hydrocarbon sub-mechanism (i.e., AramcoMech 1.3) and the KAUST $C_1$-$C_3$ alcohol sub-mechanism. Toluene and ethylbenzene sub-chemistries were updated using the alkylaromatics mechanism 2.0. The present model was tested against fuel-rich ethylene premixed flames at atmospheric pressure. The model was also compared against counterflow ethylene/propane diffusion flames to capture the fuel blending effects on PAH concentrations. The model predicted well the synergistic effect of increased PAHs with increasing propane ratio, as well as the trend that larger PAH molecules are more pronounced than smaller ones. In this study, new experiments were conducted on ethylene counterflow diffusion flames with addition of $C_2$-$C_3$ alcohols. The experimental results indicate that alcohol addition leads to increasing soot production up to a global maximum followed by decreasing soot formation with increasing alcohol mixing. Overall, the computed maximum mole fractions of A7 (i.e., a proxy for soot) for these flames are in good agreement with the experimentally observed trend. Reaction path analysis was conducted to identify key reactions contributing to PAH formation, and better understand the effects of alcohol addition to ethylene counterflow diffusion flame structure.

## Introduction

Soot and their precursors, polycyclic aromatic hydrocarbons (PAHs) have been studied extensively due to their adverse health and environmental effects [1]. Small hydrocarbon fuels ($C_1$-$C_4$) such as ethylene and propane have been studied in various flames to understand the formation of PAHs and soot. It is known that the formation and growth of PAHs are highly dependent on fuel molecular structure, and acetylene ($C_2H_2$) plays an important role in PAH growth via the sequential reactions of H-abstraction-$C_2H_2$-addition (HACA) [2]. Odd numbered carbon species such as propargyl ($C_3H_3$), cyclopentadienyl ($C_5H_5$) and indenyl ($C_9H_7$) radicals have also been identified as contributors to PAH formation. Furthermore, propargyl radical recombination reaction is considered as one of the important reactions in benzene formation [3].

Several PAH mechanisms [4, 5] have been developed and PAH growth up to five-ring aromatic species have been simulated for $C_1$-$C_2$ fuels [5]. These chemical kinetic mechanisms have been tested under various flame configurations, but they are limited to relatively small PAHs with up to four or five aromatic rings and tested mainly for single component fuels. Synergistic effects on PAH and soot formation have been observed in ethylene/propane mixture fuels [6], and chemical cross-linking effects between binary component fuels led to a clear understanding about the underlying reaction channels. Chemical reaction mechanisms for multi-component or surrogate fuels have been typically limited to small aromatic species, such as toluene and benzene. A mechanism for gasoline surrogate fuels (KM1) [7] was developed from the base mechanism [8] to account for the growth of PAHs up to coronene (A7, $C_{24}H_{12}$), and KM1 improved the prediction of PAH concentrations. A reaction mechanism for small hydrocarbon fuels ($C_1$-$C_4$) was extended to include the formation and growth of PAHs up to A7, and the mechanism (KM2) was in reasonable agreement with various experimental results [9]. A method of moments soot model was developed based on KM2 to simulate soot formation in ethylene-based counterflow diffusion flames and binary mixture with other fuels [10]; the soot model well captured the experimentally measured profiles of soot volume fraction, number density, and particle size of ethylene flames.

McNesby and co-workers [11] conducted experiments in opposed flow ethylene/air diffusion flames to understand the effects of ethanol addition to either the fuel or the oxidizer streams. They found that ethanol addition to the oxidizer stream decreases soot primarily via a thermal mechanism, while addition to the fuel stream increases soot due to a chemical mechanism that increases the methyl radical concentrations. The purpose of the present study is to expand the experimental data available on alcohol addition to ethylene diffusion flames. $C_2$ and $C_3$ alcohols were added to better understand the effects of alcohol addition on PAH and soot formation. A comprehensive kinetic model for hydrocarbon and oxygenate fuels was developed to simulate and interrogate the experimentally observations. The chemical kinetic model is compared

*Corresponding author: sungwoo.park@kaust.edu.sa

against various experimental data sets for validation.

**Experimental Methods**

In order to understand the influence of alcohol addition on ethylene diffusion flame, new experiments were conducted using counterflow diffusion flame configuration. The diameters of two opposed nozzles is 10 mm with an 8 mm separation distance. The average nozzle exit flow velocities for both the fuel and oxidizer streams were set at 15 cm/s. The oxidizer stream was composed of 27% $O_2$ and 73% $N_2$. The fuel stream was pure ethylene for the baseline case and ethanol or *n*-propanol vapor added to ethylene. To vaporize liquid fuels, the fuel supply line was heated to maintain the temperature at 180 °C and the temperature of fuel nozzle exit was maintained at 150 °C to prevent re-condensation of the pre-vaporized fuels. The temperature at the oxidizer nozzle was maintained at 25 °C. Laser-induced incandescence (LII) was used to measure the soot volume fraction.

**Kinetic Model Development**

The AramcoMech 1.3 high-temperature chemistry for the oxidation of small hydrocarbon and oxygenated (e.g., ethanol) species was utilized [12] as the base mechanism with additional reactions schemes for hydrocarbon oxidation up to benzene [13]. PAH growth reaction pathways up to coronene (A7) from KM1 [7] and KM2 [9] were then added. An *n*-propanol sub-mechanism [14] was added to simulate the effects of alcohol addition and toluene and ethylbenzene sub-chemistries were also updated using the Alkylaromatics mechanism 2.0 from Darcy et al. [13]. Additionally, PAH growth reactions initiated by propargyl ($C_3H_3$) radical addition to naphthalene (A2) leading to the formation of pyrene (A4) were added [15].

The proposed model includes 401 species and 2141 reactions. The present study follows the same notation for aromatic species with 1-7 rings (A1-A7) as [7]. Only a brief description of the proposed model is discussed herein, and readers are referred to [7, 9] for a more detailed description of PAH growth pathways. Several reactions with odd-carbon number species such as indenyl ($C_9H_7$), benzyl ($C_6H_5CH_2$), cyclopentadienyl ($C_5H_5$) and propargyl($C_3H_3$) radicals are included for PAH growth pathways along with the HACA mechanism. Most reactions for PAH growth beyond pyrene are based on the addition of acetylene ($C_2H_2$) to PAH radicals. The rate constants suggested by Kern et al. [16] are used for the decomposition of cyclopentadienyl radical to acetylene and propargyl radical. All the simulations were conducted in CHEMKIN PRO 15112 [17] using appropriate reactor modules.

**Results and Discussion**

The proposed model is first compared against fuel-rich ethylene premixed flames ($\phi$ = 3.06) data at atmospheric pressure [18]. The premixed flame simulation was performed using the PREMIX module in CHEMKIN PRO [17] with the experimental temperature profile as an input boundary condition (i.e., the gas energy equation was not solved). Figure 1 shows the comparison of experimental and computed concentrations of reactants ($C_2H_4$ and $O_2$), major products (CO, $CO_2$, $H_2$, and $H_2O$), and acetylene. The present model shows good agreement with experimental data, although $C_2H_2$ concentrations are slightly under-predicted. Experimental and kinetic modeling simulations for benzene and other PAH species are shown in Figure 2. For comparison, simulation results using ABF Mech [19] and KM2 [9] were also included. The present model well captures the concentrations of large PAH molecules with results similar to those of KM2. The results from the ABF mechanism, which is mainly based on the HACA mechanism under-estimates the concentrations of A3 and A4. These results emphasize the importance of the reaction pathways involving odd carbon number species for PAH formation, in addition to the HACA mechanism, even in the small hydrocarbon flames.

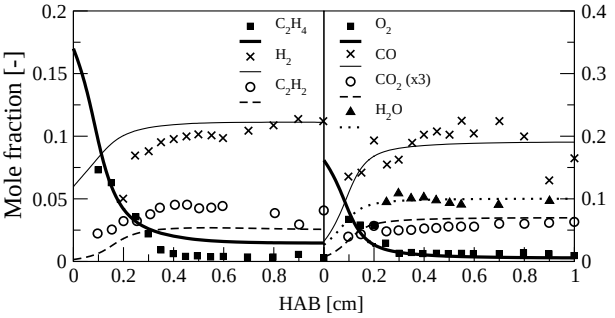


Figure 1: Comparison between experimental and calculated mole fraction of reactants, major products, and acetylene in a $C_2H_4$ premixed flame [18] (1 atm, $C_2H_4/O_2/Ar$ = 21.3/20.9/57.8)

Lee et al. [6] measured relative PAH concentrations

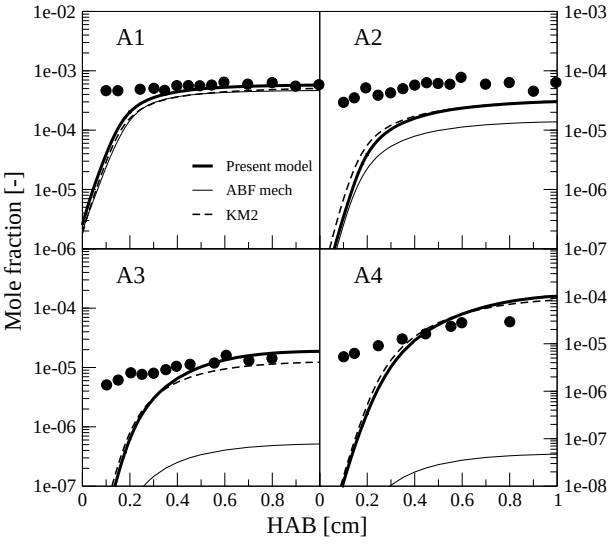


Figure 2: Comparison between experimental and calculated mole fraction of benzene and various PAHs in a $C_2H_4$ premixed flame [18] (1 atm, $C_2H_4/O_2/Ar$ = 21.3/20.9/57.8)

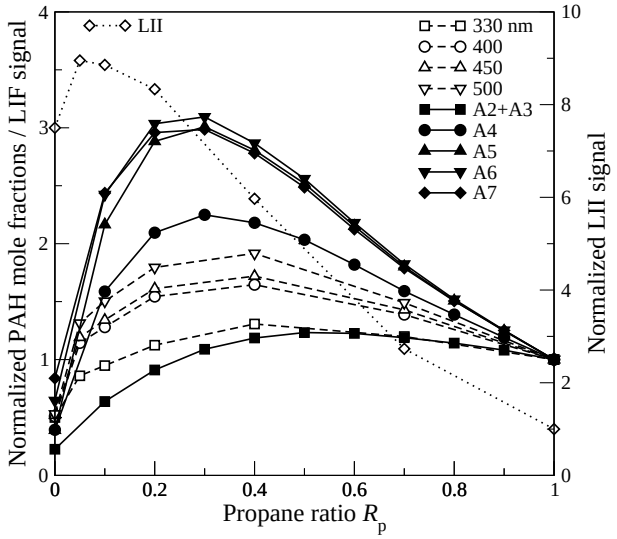


Figure 3: Comparison of normalized PAH mole fractions and LIF signals (1 atm, Fuel/ $N_2$ = 73/27, $O_2/N_2$ = 24/76, $U_0$ = 20 cm/s, experimental data from [6]).

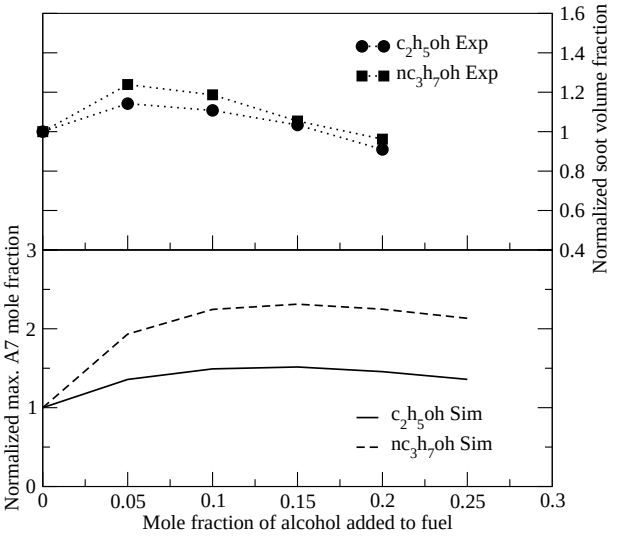


Figure 4: Comparison of normalized maximum A7 mole fractions with soot volume fraction with alcohol addition (1 atm, Fuel = 100, $O_2/N_2$ = 27/73, $U_0$ = 15 cm/s).

in counterflow ethylene/propane diffusion flames. The oxidizer stream was composed of 24% $O_2$ and 76% $N_2$, while the fuel stream was composed of a mixture of $C_2H_4$ and/or $C_3H_8$ diluted with 27 % $N_2$. The nozzle exit velocities $U_0$ were 20 cm/s with a separation distance of 1.42 cm. The propane ratio ($R_P$) was defined as the ratio of the volumetric flow rate of propane to that of the total fuel. PAH LIF signals were measured at different detection wavelengths with various $R_P$. LIF signals at higher detection wavelengths are believed to represent larger PAH molecules [9]. The PAH and soot formation zones of these flames lie on the fuel side without intensive soot oxidation, so they are well suited for the study of PAH growth. Synergistic effects were observed in the experiments and larger PAHs have higher degrees of synergistic effects. In this study, the experimental peak PAH LIF intensity at detection wavelengths from 330 to 500 nm are compared with the simulated peak mole fractions of PAHs. The present model well reproduces the experimental trends regarding synergistic effects on PAH formation, as shown in Figure 3. The predicted synergistic effect becomes more pronounced for larger PAH molecules, which agrees qualitatively with the experimental findings. According to reaction path analysis of [9], several reactions involving odd-carbon number species such as $C_9H_7$ and $C_5H_5$ contribute to the PAH growth in the flames of ethylene/propane mixtures, apart from HACA mechanism.

McNesby and co-workers [11] investigated the effects of ethanol addition to either the fuel or the oxidizer stream on soot formation in opposed flow ethylene/air diffusion flames. They found that the addition of ethanol to the fuel stream produced methyl radicals via ethanol decomposition, leading to an increase in the production of $C_4H_6$ and increased benzene production. To better understand the effects of alcohol addition to ethylene diffusion flames, new experiments were conducted on counterflow diffusion flames of ethylene with $C_2$-$C_3$ alcohol additions. The soot volume fractions were measured for ethylene flames and its binary mixture with ethanol or *n*-propanol. The experimental results indicate that alcohol addition to ethylene leads to increased soot formation, up to a global maximum, followed by decreased soot formation with increasing alcohol mixing, as shown in Figure 4. The degree of the observed synergistic effect for *n*-propanol addition is higher than for ethanol addition. The present model simulates these flames and compares the normalized maximum A7 mole fractions with the trend of soot volume fraction. This approach is justified because larger PAHs are thought to incept soot particles [20]. The proposed

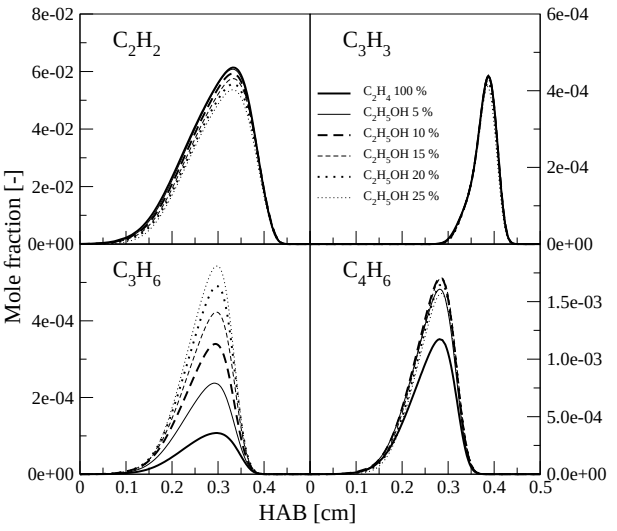


Figure 5: Comparison of major intermediate species ($C_2H_2$, $C_3H_3$, $C_3H_6$ and $C_4H_6$) for PAH formation and growth with ethanol addition (1 atm, Fuel = 100, $O_2/N_2$ = 27/73, $U_0$ = 15 cm/s).

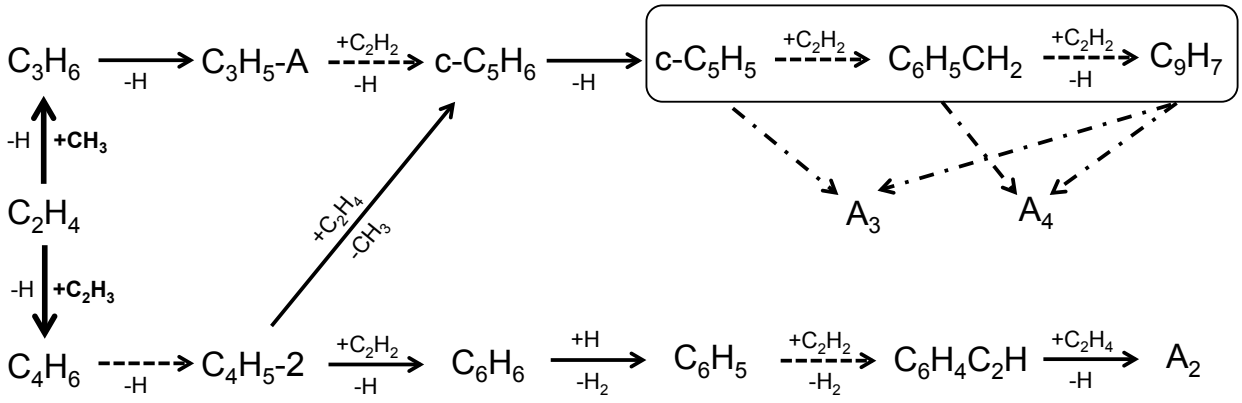


Figure 6: Overall PAH formation pathways from $C_3H_6$ and $C_4H_6$.

model quantitatively well captures the experimentally observed trend that the maximum mole fraction of A7 increases with alcohol mixing and then decreases. The degree of synergistic effect is also well predicted by the present model.

Figure 5 displays important intermediate species ($C_2H_2$, $C_3H_3$, $C_3H_6$ and $C_4H_6$) participating in PAH formation and growth with ethanol addition. The results show that acetylene ($C_2H_2$) and propargyl radical ($C_3H_3$) decrease slightly with ethanol mixing, while propene ($C_3H_6$) increases significantly as ethanol is added. Butadiene ($C_4H_6$) concentrations first increased and then decreased with increasing ethanol mixing. The results show that acetylene, which is involved in PAH growth through the HACA mechanism cannot contribute to the observed PAH synergistic effects. A reaction path analysis was carried out at 0.29 cm from the burner surface around 1290 K for 10 % ethanol addition to understand the effect of alcohol mixing on PAH formation and growth. Around 25 % of ethanol is consumed by reaction (R1) leading to the formation of ethylene and water (i.e., dehydration reaction), and 7 % by reaction (R2). These unimolecular decomposition reactions produce ethylene and increase the concentration of methyl radical in the fuel stream. Additionally, H atom abstraction of ethanol leads to the formation of acetaldehyde ($CH_3CHO$) which is eventually decomposed to CO and $CH_3$.

(R1) $C_2H_5OH$ (+ M) = $C_2H_4$ + $H_2O$ (+ M)
(R2) $C_2H_5OH$ (+ M) = $CH_3$ + $CH_2OH$ (+ M)

The methyl radical produced from ethanol decomposition enhances reactions (R3) and (R4) to increase the production of propene ($C_3H_6$). The increased vinyl radical ($C_2H_3$) from the reaction (R5) strengthens the reaction (R6) leading to the formation of $C_4H_6$.

(R3) $C_2H_4$ + $CH_3$ = $C_3H_6$ + H
(R4) $C_2H_4$ + $CH_3$ = $nC_3H_7$
(R5) $C_2H_4$ + $CH_3$ = $C_2H_3$ + $CH_4$
(R6) $C_2H_4$ + $C_2H_3$ = $C_4H_6$ + H

Figure 6 shows the overall PAH formation pathways from the increased propene and butadiene in ethylene diffusion flames with ethanol addition. Propene undergoes a series of reactions with acetylene to produce odd carbon number species such as cyclopentadienyl ($C_5H_5$), benzyl ($C_6H_5CH_2$), and indenyl ($C_9H_7$) radicals, which go towards the formation of A3 and A4. Butadiene also contributes the formation of benzene via reaction with acetylene. The proposed kinetic model mainly considers the HACA mechanism for PAH growth beyond pyrene (A4). The decreasing acetylene concentration with ethanol addition can be attributed to the non-monotonic variation in A7 concentration.

The decomposition of *n*-propanol can lead to the formation of ethylene, propene, and methyl radical by reaction (R7∼9). At 0.29 cm from the burner surface around 1260 K for 10 % *n*-propanol addition, around 21 % of *n*-propanol is consumed by reaction (R8) leading to the formation of ethylene, and 6 % via reaction (R7). The methyl produced via reaction (R9) can contribute to propene formation via reactions (R3) and (R4), and propene is pro-

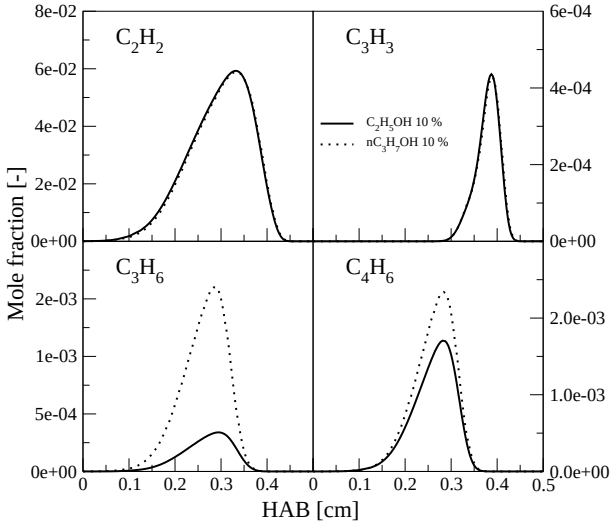


Figure 7: Comparison of major intermediate species ($C_2H_2$, $C_3H_3$, $C_3H_6$ and $C_4H_6$) between 10 % ethanol and *n*-propanol addition (1 atm, Fuel = 100, $O_2/N_2$ = 27/73, $U_0$ = 15 cm/s).

duced from the unimolecular dehydration of *n*-propanol (R7).

(R7) $nC_3H_7OH$ (+ M) = $C_3H_6$ + $H_2O$ (+ M)
(R8) $nC_3H_7OH$ (+ M) = $C_2H_5$ + $CH_2OH$ (+ M)
(R9) $nC_3H_7OH$ (+ M) = $CH_3$ + $pC_2H_4OH$ (+ M)

Figure 7 shows the comparison of intermediate species ($C_2H_2$, $C_3H_3$, $C_3H_6$ and $C_4H_6$) between 10 % ethanol and *n*-propanol addition. The results indicate that the propene and butadiene concentrations of *n*-propanol addition are much higher than ethanol addition case unlike acetylene and propargyl radical. The increased propene and butadiene play a key role to increase the concentrations of PAHs as shown in Figure 6. Therefore, the synergistic effect of PAH formation between ethanol and *n*-propanol addition to ethylene diffusion flame strongly depends on the increased concentrations of propene and butadiene.

**Conclusion**

This study proposed a chemical kinetic model for PAH growth up to A7 for ethylene flames with addition of ethanol and *n*-propanol. The proposed model was first validated against fuel-rich ethylene premixed flame data available in the literature. The proposed model also well reproduced the experimentally observed synergistic effect in counterflow ethylene/propane diffusion flames.

In order to better understand the effects of alcohol addition to PAH formation and growth, new experiments were also conducted using a counterflow ethylene diffusion flame with ethanol or *n*-propnaol added to fuel stream. New experiments on the counterflow ethylene diffusion flames with $C_2$-$C_3$ alcohol additions indicate an increase and then a decrease in soot formation with increased alcohol addition. The computed maximum mole fractions of A7 are in good agreement with the experiment. Reaction path analysis shows that alcohol addition increases the production of propene and butadiene, which in turn results in increased PAHs concentrations.

**Acknowledgment**

The authors acknowledge funding support from the Clean Combustion Research Center at King Abdulah University of Science and Technology (KAUST).

**References**

[1] H. Richter, J.B. Howard. *Prog. Energy Combust. Sci.*, 26 (2000) 565-608.

[2] M. Frenklach, J. Warnatz. *Combust. Sci. Technol.*, 51 (1987) 265-283.

[3] C.H. Wu, R.D. Kern. *J. Phys. Chem.*, 91 (1987) 6291-6296.

[4] M. Kamphus, M. Braun-Unkhoff, K. Kohse-Höinghaus. *Combust. Flame*, 152 (2008) 28-59.

[5] N.A. Slavinskaya, P. Frank. *Combust. Flame*, 156 (2009) 1705-1722.

[6] S.M. Lee, S.S. Yoon, S.H. Chung. *Combust. Flame*, 136 (2004) 493-500.

[7] A. Raj, I.D.C. Prada, A.A. Amer, S.H. Chung. *Combust. Flame*, 159 (2012) 500-515.

[8] C. Marchal, J.-L. Delfau, C. Vovelle, G. Moréac, C. Mounaïm-Rousselle, F. Mauss. *Proc. Combust. inst.*, 32 (2009) 753-759.

[9] Y. Wang, A. Raj, S.H. Chung. *Combust. Flame*, 160 (2013) 1667-1676.

[10] Y. Wang, A. Raj, S.H. Chung. *Combust. Flame*, (2014).

[11] K.L. McNesby, A.W. Miziolek, T. Nguyen, F.C. Delucia, R.R. Skaggs, T.A. Litzinger. *Combust. Flame*, 142 (2005) 413-427.

[12] W.K. Metcalfe, S.M. Burke, S.S. Ahmed, H.J. Curran. *Int. J. Chem. Kinet.*, 45 (2013) 638-675.

[13] D. Darcy, H. Nakamura, C.J. Tobin, M. Mehl, W.K. Metcalfe, W.J. Pitz, C.K. Westbrook, H.J. Curran. *Combust. Flame*, 161 (2014) 65-74.

[14] S.M. Sarathy, P. Oßwald, N. Hansen, K. Kohse-Höinghaus. *Prog. Energy Combust. Sci.*, 44 (2014) 40-102.

[15] A. Raj, M.J. Al Rashidi, S.H. Chung, S.M. Sarathy. *J. Phys. Chem. A*, 118 (2014) 2865-2885.

[16] R.D. Kern, Q. Zhang, J. Yao, B.S. Jursic, R.S. Tranter, M.A. Greybill, J.H. Kiefer. *Proc. Combust. inst.*, 27 (1998) 143-150.

[17] CHEMKIN-PRO 15112, Reaction Design, San Diego, 2011.

[18] M.J. Castaldi, N.M. Marinov, C.F. Melius, J. Huang, S.M. Senkan, W.J. Pit, C.K. Westbrook. *Proc. Combust. inst.*, 26 (1996) 693-702.

[19] J. Appel, H. Bockhorn, and M. Frenklach. *Combust. Flame*, 121 (2000) 122-136.

[20] A. Raj, M. Sander, V. Janardhanan, and M. Kraft. *Combust. Flame*, 157 (2010) 523-534.